Dielectrophoretic cell trapping for improved surface plasmon resonance imaging sensing

Marion Costella, Quentin Avenas, Marie Frénéa-Robin, Julien Marchalot, Pascal Bevilacqua, Paul Charette, Michael Canva

Dielectrophoretic cell trapping for improved Surface Plasmon Resonance Imaging sensing

M.Costella[1,2], Q. Avenas[1,2], M. Frénéa-Robin[1], J. Marchalot[1], P. Bevilacqua[1], P. Charette[2,3], M. Canva[2,3]

[1] Université de Lyon, École Centrale de Lyon, Université Claude Bernard Lyon 1, INSA Lyon, CNRS, Ampère,-F-69130, Écully, France

[2] Laboratoire Nanotechnologies Nanosystèmes (LN2) - CNRS UMI-3463, Université de Sherbrooke, École Centrale de Lyon - Sherbrooke, Canada

[3] Institut Interdisciplinaire d'Innovation Technologique (3IT) - Université de Sherbrooke- Sherbrooke, Canada

Corresponding author: Marion Costella

Marion.Costella@USherbrooke.ca

3000 Boulevard de l'Université

J1K 0A5 Sherbrooke, Canada

https://orcid.org/0000-0002-4897-4790

Received: 10 15, 2018; Revised: 02 21, 2019; Accepted: 02 21, 2019

This article has been accepted for publication and undergone full peer review but has not been through the copyediting, typesetting, pagination and proofreading process, which may lead to differences between this version and the Version of Record. Please cite this article as doi: 10.1002/elps.201800439.

List of abbreviations

AC: Alternating current

ACEO: Alternating current electro-osmosis

EOT: extraordinary optical transmission

IDE: Interdigitated electrodes

nDEP: negative dielectrophoresis

NIR: Near-infrared

pDEP: positive dielectrophoresis

RIU: Refractive index unit

ROI: Region of interest

TE: Transverse electric

TM: Transverse magnetic

SPR: Surface plasmon resonance

SPRI: Surface plasmon resonance imaging

UV: Ultraviolet

Keywords: biosensing instrumentation, dielectrophoresis, electro-osmosis, surface plasmon resonance, top-bottom electrodes

Abstract

The performance of conventional surface plasmon resonance (SPR) biosensors can be limited by the diffusion of the target analyte to the sensor surface. This work presents an SPR biosensor that incorporates an active mass-transport mechanism based on dielectrophoresis (DEP) and electroosmotic flow to enhance analyte transport to the sensor surface and reduce the time required for detection. Both these phenomena rely on the generation of AC electric fields that can be tailored by shaping the electrodes that also serve as the SPR sensing areas. Numerical simulations of electric field distribution and microparticle trajectories were performed to choose an optimal electrode design. The proposed design improves on previous work combining SPR with DEP by using face-to-face electrodes, rather than a planar interdigitated design. Two different top-bottom electrode designs were experimentally tested to concentrate firstly latex beads and secondly biological cells onto the SPR sensing area. SPR measurements were then performed by varying the target concentrations. The electrohydrodynamic flow enabled efficient concentration of small objects (3 μm beads, yeasts) onto the SPR sensing area, which resulted in an order of magnitude increased SPR response. Negative dielectrophoresis was also used to concentrate HEK293 cells onto the metal electrodes surrounded by insulating areas, where the SPR response was improved by one order of magnitude.

Color online: See article online to view Figs. 1–5 in color.

1. Introduction

Surface Plasmon Resonance (SPR) biochips are highly sensitive, real-time and label-free sensors used for surface-based study of biomolecular interactions and detection of biological objects in fluid media [1,2]. They have become standard tools for chemical and biological sensing, and have found many practical applications including medical diagnosis [3]–[6], food safety [7], [8], environmental monitoring [9], [10], and pharmaceutical research [11]. Recent microfabrication advances have enabled SPR devices to become portable [12]–[14]. SPR sensors make use of the evanescent field of a guided electromagnetic mode at a metal/dielectric interface. When using a prism for input/output light coupling (Kretschmann configuration), the mode is excited at a specific wavelength and angle of incidence where transverse magnetic (TM) incident light is resonantly coupled to the surface plasmon mode and the reflected output light intensity is thereby minimized. Local changes in the dielectric close to the metal/dielectric interface (within ~200 nm for visible and near-infrared systems) induced by molecular binding or the presence of biological objects modify the mode properties and the associated coupling conditions. As a result, biomolecular activity close to the sensor surface can be monitored by tracking changes in light output intensity and/or resonance conditions. By using an imaging device (camera), monitoring of biomolecular activity can be spatially resolved on the sensor surface (metal/dielectric interface).

During the last decades, SPR biosensors have been extensively studied and their detection threshold is now close to their theoretical limit [15]. The performance level of current SPR biosensors, estimated as the smallest detectable refractive index change, reaches 10^{-7} refractive index units (RIU) [16]. However, the detection of analytes suspended in a medium not only depends on the

sensor performance but also on mass transport of analytes to the sensor surface. Indeed, the sensitivity of current SPR biosensors is often limited by diffusion-limited mass transport [17]. This limit can be overcome by increasing the analyte concentration near the sensor surface with active mass transport, for example with dielectrophoresis (DEP) and AC electroosmotic (ACEO) flow [18]–[20]. The biochip proposed here uses a microstructured gold/dielectric film, similar in thickness and optical properties to those used in conventional SPR biochip systems, for both the SPR sensing surface and the electrodes used for control of the active mass transport by DEP and ACEO.

DEP results from the interaction between a polarizable particle and a non-uniform electric field. The dielectrophoretic force applied on a spherical particle of radius *r* in a fluid medium can be expressed as:

$$\langle F_{DEP} \rangle = 2\pi\varepsilon_m r^3 Re(CM) \nabla E_{rms}^2 \quad (1)$$

where ε_m is the permittivity of the fluid medium, E_{rms} is the root mean square of the electric field amplitude, and *Re(CM)* is the real part of the Clausius-Mossotti (*CM*) factor, given by:

$$CM = \frac{\varepsilon_p^* - \varepsilon_m^*}{\varepsilon_p^* + 2\varepsilon_m^*} \quad (2)$$

where ε_p^* and ε_m^* are the complex permittivity of the particle and the fluid medium, respectively.

Depending on the polarization contrast with the fluid medium, the particle can either be attracted to high electric field zones (positive DEP, positive *CM* factor) or pushed towards weak field zones (negative DEP, negative *CM* factor). Dielectrophoresis requires an electric field gradient, typically produced by shaping electrodes and distorting field profiles. An alternative is to combine insulating

structures with recessed electrodes to produce the electric field gradient and trap objects following the principle of insulator-based dielectrophoresis (iDEP) [21].

Electroosmotic flow occurs when the tangential component of the electric field moves ions in the ionic double layer at the metal/medium interface [22]. While positive dielectrophoresis typically attracts objects to the edge of electrodes, electro-osmosis is able to drag them towards the center of the electrodes [23], which facilitates SPR detection.

Barik et al. have shown [24] that nanohole-enhanced dielectrophoresis and electro-osmosis significantly lower the detection limit of protein like BSA, as measured by exploiting extraordinary optical transmission (EOT). More recently, other groups have demonstrated the combination of plasmonics with active mass transfer by using ACEO to concentrate biomolecules on gold nanoparticles [25], photothermal heating to trap polystyrene beads on a plasmonic nanostructured substrate [26], or dielectrophoresis to concentrate beads or bacteria near a gold-coated optical fiber tip [27]. However, these techniques need nanofabrication steps which require expensive equipment and long manufacturing processes. Dielectrophoresis and ACEO combined with plasmonics have also been used to enhance fluorescently-labeled biological substance detection [28]–[30]. To the best of our knowledge, Galvan et al. [31] were the first to publish work on combining prism-based SPR sensing (the most widely-used SPR configuration, i.e. the Kretschmann configuration) with DEP-assisted active mass transport. In their work, the electric field is created using interdigitated electrodes (opposite polarity electrodes are in the same plane).

In this work, we propose an improved configuration for active mass transport with SPR based on face-to-face electrodes that significantly enhances the target collection ability by both DEP and ACEO. Results from both numerical simulations and experimental measurements with latex microbeads and biological cells are presented. Such DEP-SPR biochips can easily be fabricated with

standard low-cost photolithography techniques and could therefore be widely distributed and used when needed with minor modifications to existing SPR systems

2. Materials and methods

2.1 SPRI optical set-up

The layout of the SPR-DEP system is depicted in Figures 1a and 1b. The major optical components around the biochips are the light source (collimated 740 nm fibered LED, Thorlabs, M740F2), a prism coupler (SF10 prism) and a detector (camera). The SPR biochips are mounted on the prism in the Kretschmann configuration [32]. The optical contact between the prism and the SPR biochip is made using index matching oil. A custom-made device (Figure 1a) clamps together the different parts of the biochip (bottom glass slide with electrode, top-side counter electrode, and fluidic chamber in between) and allows the connection of electrodes to a signal generator (Stanford Research Systems, DS345).

Figure_1

The microfluidic channel is cut out from a 200 µm thick PDMS film obtained by spin coating, which is used as a spacer between the electrode and the counter electrode. Another thick PDMS block (0,5 cm) is bounded to the ITO-coated glass slide with O_2 plasma. It distributes the pressure on the channel when the screws are tightened. Contact pins soldered to the circuit board provide electrical contacts to the electrode and the counter electrode. The electric signal is transferred from the bottom board to the top board through the screws. A motorized rotation stage (Thorlabs) controls the incidence angle and the detector position. After reflection at the metal/fluid, the light beam goes through an objective (Mitutoyo, x5 or x10), and a polarizing cube beam splitter to separate TE and

TM images. TE and TM images are acquired using two CCD cameras (Allied Vision, Mako, G234B POE). The SPR signal is extracted from the TM image light intensity.

2.2 DEP-SPRI biochip fabrication

As shown in Figure 1a and 1b, the chosen electrode configuration for dielectrophoresis is a face-to-face (or top-bottom) configuration. The top electrode is an ITO coated glass slide (8-12 Ω/sq, Sigma-Aldrich). The bottom electrode is a microscope glass slide purchased from Fisher Scientific, coated with a 3 nm chromium adhesion layer, and a 48 nm gold layer by evaporation. Two configurations are proposed for the bottom electrode. In the "dielectric structured" configuration (Figure 1c), a 150 nm SiO_2 insulation layer is deposited by plasma-enhanced chemical vapor deposition (PECVD) onto the gold film at 300°C and 1 mTorr. Then, openings are formed in the SiO_2 layer using wet etching. For this purpose, AZ1512 (MicroChemicals) positive photoresist is first spin-coated on the sample and post-baked at 110°C for 3 min. Then, the photoresist is exposed to UV light (OAI 200, Optical Associated Inc.) through an acetate mask superposed on the sample, before being developed using MF319 developer (Shipley).

Acetate photomasks were used during this step to reduce the cost of the process and allow for the comparison of a wide variety of electrode designs. Finally, the SiO_2 layer is etched with buffered oxide etch (BOE 6:1) prior to removal of the resist mask using acetone.

In the "metal structured" configuration (Figure 1d), the gold film is etched to electrically insulate some zones where cells will be trapped by negative dielectrophoresis. The wet etching process is similar to the one previously described, except that the gold layer and the chromium adhesion layer are etched using Gold Etchant TFA and Chromium Etchant (Transene Company, Inc.), respectively.

2.3. Cell and particle preparation

Latex beads solutions (3 µm diameter, Polyscience) were prepared by diluting the stock solution with DI water to obtain a final concentration of 36.5×10^6 particles/mL. Human embryonic kidney cells (HEK293) were grown at 37°C under 5% CO_2 in Dulbecco's modified Eaglemedium (DMEM), with 10% fetal bovine serum (FBS), 100 µg/mL streptomycin, and 100 units/mL penicillin. Before each DEP and SPR experiment, cells were detached with a trypsin solution (phosphate-buffered saline containing 0.05% trypsin and 0.02% EDTA) and resuspended in a low conductivity medium (8.5% sucrose (w/v) and 0.3% dextrose (w/v) in DI water).

2.4. DEP-SPRI measurement protocol

On the SPR optical bench, cameras and light source are fixed on a rotation stage to control the light incidence and reflection angles. The whole system is controlled using the software developed in the LabVIEW environment. Before each measurement, buffer solution is injected in the microfluidic chamber using a syringe pump. Then, the working angle ϑ_0 at fixed wavelength is determined from an angular scan. The reflectivity as function of the incidence angle is measured and the working angle θ_0 is chosen as the angle of incidence for which the reflectivity variation is maximal. This angle guarantees the maximal sensitivity of the sensor. After stabilisation of the SPR signal, analytes are injected. Then, after a certain time necessary to the signal stabilization, AC voltage is applied for the dielectrophoretic trapping. Throughout the measurement process, transverse magnetic (TM) and transverse electric (TE) images are recorded. Intensity variation in the TM image corresponds to optical index changing near the metallic film, which reveals the presence of beads or biological objects. Several regions of interest (ROI) are defined on the TM image, including DEP electrodes, and reference electrode. The temporal evolution of ROI's average pixel value is monitored by post-

processing thanks to the ImageJ software and the Time Series Analyzer V3 plugin. It corresponds to the SPR signal.

To compensate for brightness differences between measurements, all SPR signals are normalized setting their initial value to 1. The reference electrode is an unpatterned, non-polarized gold film. The SPR signal for this zone corresponds to that detected by a classical SPR biochip.

2.5 Optical microscopy setup

Axiocam MRM camera mounted on a Zeiss Axiovert 200 inverted microscope was used for bright field imaging. Similar electrical setup and energy supply were used in both SPR and bright field imaging.

3. Results and discussion

3.1 Numerical simulations for electrode design choice

The SPR signal enhancement of microparticles under DEP forces and ACEO flow generated by coplanar interdigitated electrodes has been previously studied in our group and reported elsewhere [33]. However, with this configuration, particles far away from the electrodes will be less responsive to the DEP forces, due to the rapid electric field decay with the distance from the electrodes.

Figure_2

Face-to-face electrodes can be used as an alternative, since they generate a strong electric field in the whole height of the channel. Dead DEP collection volumes can thus be avoided [34], [35]. The expected consequence would be a greater efficiency of particle trapping. To quantify this effect, simulations of particles trajectories were performed both for coplanar and face-to-face electrodes using a Comsol Multiphysics 5.3a 3D model and the add-on *AC/DC*, *Microfluidics* and *Particle Tracing* modules. Electric field models of channel cross-sections corresponding to the "dielectric structured" and the "metal structured" configuration are depicted in Figure 2a and 2b. Figure 2c and 2d represent the CM factor for 3 µm latex beads and HEK293 cells calculated with MyDEP software [36]. Electric properties of HEK293 cells present in the MyDEP database were used [37]. Electric properties values of latex beads used in this paper were previously studied by Suzuki et al. [38] in similar conditions (DI water).

The thickness of electrodes and dielectric layer were considered as negligible. First, a frequency study was used to solve the electrical problem in the *Electric Current* interface of the *AC/DC* module using Eqs. 3-6:

$$\boldsymbol{\nabla}.\boldsymbol{J} = Q_J \tag{3}$$

$$\boldsymbol{E} = -\boldsymbol{\nabla}V \tag{4}$$

$$\boldsymbol{J} = \sigma\boldsymbol{E} + j\omega\boldsymbol{D} + \boldsymbol{J_e} \tag{5}$$

$$\boldsymbol{D} = \varepsilon_0\varepsilon_r\boldsymbol{E} \tag{6}$$

where Q_v, σ, ω, **D**, V, $\mathbf{J_e}$, $\varepsilon_0, \varepsilon_r$ are charge density, conductivity, angular frequency, electric displacement field, applied potential, external generated current density, permittivity of the vacuum, and relative permittivity of the medium, respectively. Q_v and $\mathbf{J_e}$ were set equal to zero in our calculation. Electrodes were considered as equipotential surfaces. The potential of the bottom electrode was set at 5V, and the potential of the top electrode was set at -5V. Electrical insulating boundary conditions were set on the fluidic chamber's walls. Then, the gravity force, the drag force and the dielectrophoretic force were modeled using pre-calculated forces available in the *Particle Tracing* module. In this module, Newton's second law of movement (Eq. 7) is solved for each particle:

$$\frac{d}{dt}(m_p \boldsymbol{v}) = \boldsymbol{F} \qquad (7)$$

Where m_p is the mass of the particle, $\boldsymbol{v}$ is its velocity, and $\boldsymbol{F}$ is the sum of the forces applied on the particle (DEP force, drag force and gravity force). This model was meshed using a free triangular configuration on the bottom electrodes with a minimum element size of 0.05 µm and a maximum element size of 1 µm. The rest of the fluidic chamber was meshed using a free tetrahedral configuration with a minimum size of 1 µm. The *Particle Tracing* study was computed in a time-dependent mode to predict the particle trajectory inside the fluidic chamber.

Figure_3

Electric field repartition for each configuration is depicted in Figure 3a, 3b and 3c for a 10 V_{pp} applied voltage. For the nDEP model, a floating potential condition is defined on the central square depicted in Figure 1d. A 35 seconds temporal study describes the trajectory of 200 particles randomly distributed in the 200 µm channel height. The particle's position after 25 seconds is represented in

Figure 3d, 3e, and 3f. SPR signal grows with the density of analytes trapped at the surface of the sensor. The number of particles trapped on electrodes for the coplanar and face-to-face electrodes versus time is represented in Figure 3g. These simulations reveal a stronger concentration of cells on gold for the face-to-face electrodes than for coplanar electrodes, especially in the pDEP case. In this case, particles are attracted on high electric field zones, at the boundary between gold and SiO_2 layer. This is not ideal for SPR detection. However, this model does not take account ACEO flow, which brings objects on the center of electrodes and allows a better detection. As the surface of electrodes is equivalent for both configurations, the density difference is due to the dielectrophoretic force, and not to a surface effect. The trapping efficiency of the interdigitated electrodes could be enhanced by optimizing some parameters such as the gap between the electrodes and their width, or the voltage. Electroosmotic flow could also be exploited to drag the particles towards the trapping sites. However, our simulations tend to show that the face-to-face configuration may be particularly interesting for the targeted application. For this reason and in the following experimental section, all the SPR-DEP electrodes are in this configuration.

3.2 DEP and ACEO experimental trapping

The dielectrophoretic behavior of 3 µm latex particles and HEK293 cells was investigated. In this paper, two approaches are described. In the first one ("dielectric structured"), following the concept of iDEP [39], an insulation layer is patterned to obtain openings on gold, as shown in Figure 1c. Figure 4a represents the 3 µm latex beads position after few minutes under a 1 V_{rms} and 1 kHz AC voltage in DI water. Under these conditions, the Clausius-Mossotti factor predicts positive dielectrophoresis (Figure 2c) and the beads are attracted to the electric field maxima located at the boundary between insulated zones (SiO_2) and conductive zones (gold). As the top and the bottom electrodes are asymmetric, the electric field has a tangential component that sets in motion the mobile ions in the electric double layer. This results in an electro-osmotic (ACEO) flow, which is non-negligible in the frequency range used [40]. In the "dielectric structured" configuration, the electro-

osmotic flow leads to vortexes at the edge of the electrodes [41]. This flow drags the particles from the edge of the electrode to its center, which is an advantage for SPR sensing. Figure 4b shows that the beads accumulate on the electrode surface when the voltage is applied. Particle arrangement shows a crystal structure. When the voltage is switched off, beads are randomly dispersed. We observe that ACEO flow efficiently concentrates 3 µm latex beads and yeasts cells. For bigger objects such as HEK293 cells (R = 7,5 µm), the drag force induced by the EHD flow is too weak compared with the pDEP force to bring objects to the center of the electrodes. As the DEP force grows as R^3 (R being the radius of the particle), the pDEP force is enough to maintain beads on the edge of the electrodes, despite the electroosmotic flow. This configuration is therefore not well adapted for the detection of cells by SPR. In the second approach ("metal structured" configuration), the gold film is directly patterned as displayed in Figure 1d. nDEP trapping of HEK293 is studied in this configuration. To reach a physiological value of osmolality in a low conductivity medium, cells are suspended in DI water supplemented with sucrose/dextrose. At 5 kHz, cells experienced negative dielectrophoresis. As predicted by the CM factor (Figure 2d), cells are attracted towards electric field minima located on the electrically isolated gold squares. Due to the floating potential of the isolated gold squares, electric field minima are not located perfectly at the center of these islets. As a result, cells are not perfectly centered on those zones on which SPR sensing is being performed. After a few minutes, all cells are trapped, as shown in Figure 5a.

3.3 SPR sensing enhancement

SPR-based sensors are highly sensitive to changes in the refractive index near the metallic film. The application of an external potential difference to the gold film might lead to its oxidation [42], or modify the charges distribution in the double layer at the metal-liquid interface [43]. This could result in an SPR angular shift, which would depend on the voltage and the frequency applied. In this

study, the SPR angular shift due to the AC voltage is negligible compared with the angular shift induced by the detection of a biological object.

3.3.1 "Dielectric structured" configuration

Figure 4c represents the TM image corresponding to Figure 4a. To avoid detrimental optical effects, the plasmon propagation direction is aligned along the rectangular electrodes. As shown in Figure 4a and 4b, pDEP attracts the latex beads on 100 µm wide openings on SiO_2. Therefore, they are concentrated at the center of the electrodes thanks to the ACEO flow.

Figure_4

Figure 4d shows the temporal evolution of the normalized SPR signal on the DEP electrode after injecting the beads, powering on the voltage and washing with DI water. The SPR signal after bead injection is the one obtained with a classical SPR sensor. As soon as the voltage is applied, bead arrival on electrodes induces a strong signal enhancement. Out of the saturation regime, this signal jump is linked to the initial bead concentration in the solution. Then, the voltage is switched off and the SPR signal on electrodes decreases. This is due to the bead density drop which corresponds to the switch between a crystal-like and a random organization of beads. The predominance of electroosmotic flow on the dielectrophoretic force makes this configuration particularly interesting for small objects (such as bacteria) trapping and detection.

3.3.2 "Metal structured" configuration

The image of the “metal structured” gold film is displayed in Figure 5b. Figure 5c represents the temporal evolution of the SPR signal on a patterned gold film and on a planar electrode similar to a classical SPR sensor. After cell injection, a 7 V_{pp} and 5 kHz signal is applied. At this frequency, the Clausius-Mossotti factor predicts negative dielectrophoresis for HEK293 cells in a low conductivity medium (Figure 2d). The arrival of cells on electrodes is monitored by the SPR signal rise, slower than in the precedent configuration because the nDEP force is weaker than the pDEP force.

Figure_5

Indeed, the Clausius-Mossotti factor ranges from -0.5 to 1, which means that at the optimal frequencies conditions, pDEP force is always greater than nDEP force. However, nDEP presents interesting properties for the manipulation of biological objects. As cells are trapped at electric field minima, their membrane is less electrically stressed than by pDEP trapping. The temporal evolution of the SPR signal plotted in Figure 5c shows that nDEP provides an SPR signal significantly stronger than the maximal signal attainable with a classical SPR biochip.

Indeed, the Clausius-Mossotti factor ranges from -0.5 to 1, which means that at the optimal frequency condition, the pDEP force is always greater than the nDEP force. However, the nDEP presents interesting properties for the manipulation of biological objects. As cells are trapped at electric field minima, their membrane is less electrically stressed than by pDEP trapping. The temporal evolution of the SPR signal plotted in Figure 5c shows that nDEP provides an SPR signal significantly stronger than the maximal signal attainable with a classical SPR biochip.

4. Concluding remarks

Two different designs of a dielectrophoresis-assisted SPRI biochip structure dedicated to the detection of biological objects were considered. Using simulation tools, we numerically demonstrated the greater particle/target collection capabilities of “face to face” electrodes compared with “coplanar” electrodes.

In this “face-to-face” electrodes case, we studied two different types of structures, respectively adapted to negative dielectrophoresis and positive dielectrophoresis. The “dielectric structured” design exploits ACEO and positive dielectrophoresis to center small particles on electrodes, whereas the “metallic structured” design is intended to trap objects on a non-connected area of the metal film by negative dielectrophoresis. Both behaviors were experimentally demonstrated and exhibited significant signal in conditions whereas without the DEP contribution none was obtained.

Furthermore, it is worth pointing out that such structurally modified biochip components can easily be integrated on existing academic or commercial SPR devices and therefore be routinely used to allow a faster and more sensitive target detection for many application whenever needed. Such dielectrophoretic-assisted trapping of analytes is particularly interesting for the detection of ultra-low target concentrations, where no detection would be possible within a given allotted time using classical transport-limited SPR biochip reader systems.

As is well known, classical biochips are usually functionalized with a surface chemistry for the selective detection of specific targets. Combined with such surface chemistry, such DEP-SPRI approach will open up new applications making use of rapid and low-detection SPRI sensor instruments. SPR sensors.

Acknowledgements

This work was supported by doctoral scholarships from MITACS and IDEX Lyon. LN2 is an international laboratory (Unité Mixte Internationale UMI 3463) jointly managed by French CNRS and the Université de Sherbrooke as well as Université de Lyon (ECL, INSA de Lyon, CPE) and the Université Grenoble Alpes (UGA). Authors thank A. Sabac, T. Deschamps, A. Belarouci and the NanoLyon platform for the thin film deposition. The authors also thank U. Froehlich and S. Touchette for cell culture.

The authors have declared no conflict of interest.

5 References

[1] Dudak, F. C., Boyaci, I. H., *Biotechnol. J.* 2009, 4, 1003–1011.

[2] Wong, C. L., Olivo, M., *Plasmonics* 2014, 9, 809–824.

[3] Fu, E., Chinowsky, T., Nelson, K., Yager, P., in *Handbook of Surface Plasmon Resonance* (Eds.: Schasfoort, R. B. M., Tudos, A. J.), RCS Publishing, Cambridge UK 2008*,* pp. *313–332*.

[4] Chung, J. W., Kim, S. D., Bernhardt, R., Pyun, J. C., *Sens. Actuators B* 2005, 111–112, 416–422.

[5] Yanase, Y., Sakamoto, K., Kobayashi, K., Hide, M., *Opt. Mater. Express* 2016, 6, 1339.

[6] Pawula, M., Altintas, Z., Tothill, I. E., *Talanta* 2016, 146, 823–830.

[7] Piliarik, M., Párová, L., Homola, J., *Biosens. Bioelectron.* 2009, 24, 1399–1404.

[8] Ashley, J., Piekarska, M., Segers, C., Trinh, L., Rodgers, T., Willey, R., Tothill, I. E., *Biosens. Bioelectron.* 2017, 88, 109–113.

[9] Herranz, S., Bocková, M., Marazuela, M. D., Homola, J., Moreno-Bondi, M. C., *Anal. Bioanal. Chem.* 2010, 398, 2625–2634.

[10] Brulé, T., Granger, G., Bukar, N., Deschênes-Rancourt, C., Havard, T., Schmitzer, A. R., Martel, R., Masson, J. F., *Analyst* 2017, 142, 2161–2168.

[11] Olaru, A., Bala, C., Jaffrezic-Renault, N., Aboul-Enein, H. Y., *Crit. Rev. Anal. Chem.* 2015, 45, 97–105.

[12] Liu, Y., Liu, Q., Chen, S., Cheng, F., Wang, H., Peng, W., *Sci. Rep.* 2015, 5, 1–9.

[13] Tokel, O., Yildiz, U. H., Inci, F., Durmus, N. G., Ekiz, O. O., Turker, B., Cetin, C., Rao, S., Sridhar, K., Natarajan, N., Shafiee, H., Dana, A., Demirci, U., *Sci. Rep.* 2015, 5, 1–9.

[14] Trzaskowski, M., Napiórkowska, A., Augustynowicz-Kopeć, E., Ciach, T., *Sens. Actuators B* 2018, 260, 786–792.

[15] Piliarik, M., Homola, J., *Opt. Express* 2009, 17, 16505.

[16] Homola, J., *Chem. Rev.* 2008, 108, 462–493.

[17] Sheehan, P. E., Whitman, L. J., *Nano Lett.* 2005, 5, 803–807.

[18] Hoettges, K. F., Mcdonnell, M. B., Hughes, M. P., *J. Phys. D. Appl. Phys.* 2003, 36, 101–104.

[19] Li, S., Ren, Y., Jiang, H., *RSC Adv.* 2014, 4, 9064–9071.

[20] Salari, A., Thompson, M., *Sens. Actuators B* 2018, 255, 3601–3615.

[21] Lapizco-Encinas, B. H., Simmons, B. A., Cummings, E. B., Fintschenko, Y., *Anal. Chem.* 2004, 76, 1571–1579.

[22] González, A., Ramos, A., Green, N. G., Castellanos, A., Morgan, H., *Phys. Rev. E* 2000, 61, 4019–4028.

[23] Oh, J., Hart, R., Capurro, J., Noh, H. (M.), *Lab Chip* 2009, 9, 62–78.

[24] Barik, A., Otto, L. M., Yoo, D., Jose, J., Johnson, T. W., Oh, S. H., *Nano Lett.* 2014, 14, 2006–2012.

[25] Song, Y., Chen, P., Chung, M. T., Nidetz, R., Park, Y., Liu, Z., McHugh, W., Cornell, T. T., Fu, J., Kurabayashi, K., *Nano Lett.* 2017, 17, 2374–2380.

[26] Ndukaife, J. C., Mishra, A., Guler, U., Nnanna, A. G. A., Wereley, S. T., Boltasseva, A., *ACS Nano* 2014, 8, 9035–9043.

[27] Tai, Y., Chang, D., Pan, M., Huang, D., Wei, P., *Sensors* 2016, 16, 1–9.

[28] Kuroda, C., Iizuka, R., Ohki, Y., Fujimaki, M., *Jpn. J. Appl. Phys.* 2018, 57, 1–5.

[29] Velmanickam, L., Fondakowski, M., Lima, I. T., Nawarathna, D., *Biomicrofluidics* 2017, 11, 044115.

[30] Kuroda, C., Ohki, Y., Fujimaki, M., *IEEE Conference on Electrical Insulation and Dielectric Phenomenon*, Texas 2017, 253–256.

[31] Galvan, D. D., Parehk, V., Liu, E. J., Liu, E.-L., Yu, Q., *Anal. Chem.* 2018, 90, 14635–14642.

[32] Kretschmann, E., Raether, H., *Z. Naturforsch.* 1968, 23, 2135–2136.

[33] Avenas, Q., Moreau, J., Costella, M., Maalaoui, A., Souifi, A., Charette, P., Marchalot, J., Frénéa-Robin, M., Canva, M., *Electrophoresis* 2019.

[34] Wang, L., Flanagan, L. A., Jeon, N. L., Monuki, E., Lee, A. P., *Lab Chip* 2007, 7, 1114–1120.

[35] Abdallat, R. G., Ahmad Tajuddin, A. S., Gould, D. H., Hughes, M. P., Fatoyinbo, H. O., Labeed, F. H., *Electrophoresis* 2013, 34, 1059–1067.

[36] Cottet, J., Fabregue, O., Berger, C., Buret, F., Renaud, P., Marie Frénéa-Robin, *Biophys. J.* 2019, 116, 12–18.

[37] Zimmerman, D., Kiesel, M., Terpitz, U., Zhou, A., Reuss, R., Kraus, J., Shenk, W. A., Bamberg, E., Sukhorukov, V. L., *J. Membr. Biol.* 2008, 221, 107–121.

[38] Suzuki, M., Yasukawa, T., Mase, Y., Oyamatsu, D., Shiku, H., Matsue, T., *Langmuir*, 2004, 20, 11005–11011.

[39] Iliescu, C., Xu, G., Tong, W. H., Yu, F., Bălan, C. M., Tresset, G., Yu, H., *Microfluid. Nanofluid.* 2015, 19, 363–373.

[40] Green, N. G., Ramos, A., González, A., Morgan, H., Castellanos, A., *Phys. Rev. E* 2002, 66,

26305.

[41] Islam, N., Lian, M., Wu, J., *Microfluid. Nanofluid.* 2007, 3, 369–375.

[42] Lioubimov, V., Kolomenskii, A., Mershin, A., Nanopoulos, D. V, Schuessler, H. A, *Appl. Opt.* 2004, 43, 3426–3432.

[43] Lopatynskyi, A. M., Lopatynska, O. G., Guiver, M. D., Poperenko, L. V, Chegel, V. I., *Semicond. Phys., Quantum Electron. Optoelectron.* 2008, 11, 329–336.

Figure captions:

Figure 1: Scheme of the top-bottom electrode and the fluidic channel in the circuit board (a). Picture of the setup mounted on a prism in the Kretschmann configuration (b). Two configurations of bottom electrode are studied: "dielectric structured" electrode (c) and "metal structured" electrode (d).

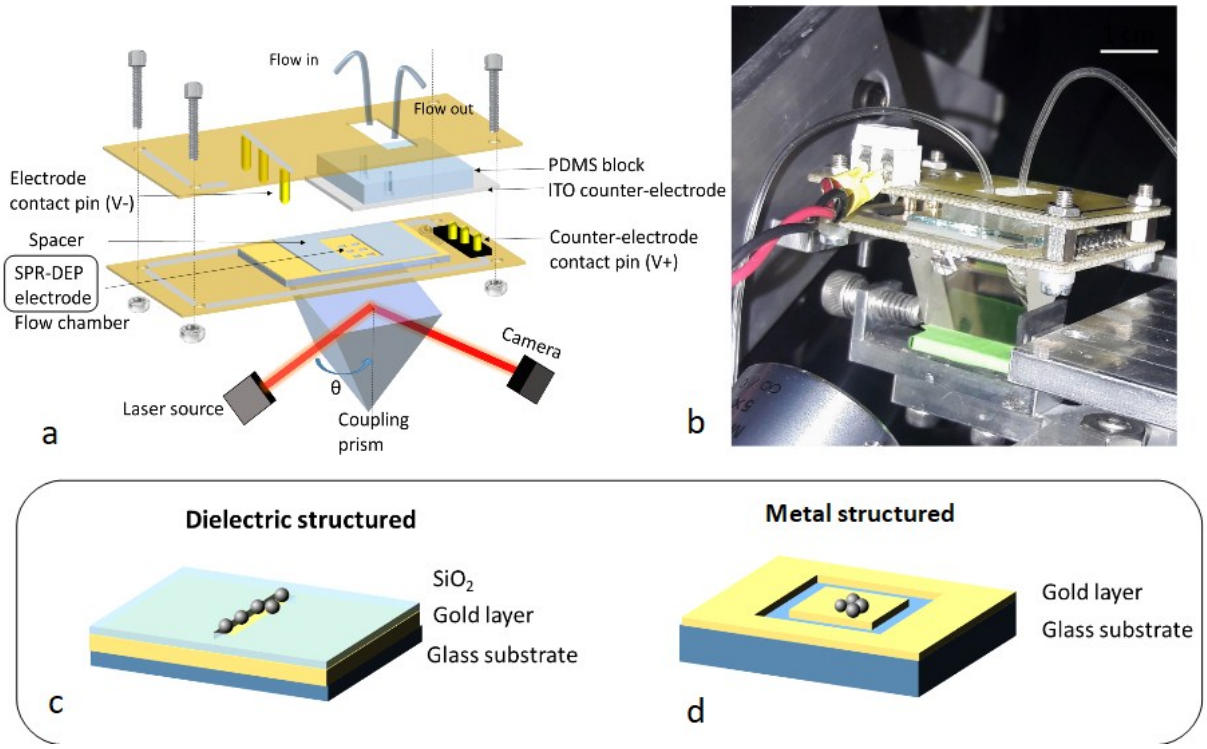

Figure 2: Electric field lines for the "dielectric structured" configuration (a) and the "metal structured" configuration (b). Clausius-Mossotti factor calculated for latex beads ($\varepsilon_p = 2.56$, $\sigma_p = 2.10^{-3}$ S/m) in DI water (c), and cells modeled by a single shell particle (radius = 7.5 µm, $\varepsilon_{int} = 71$, $\varepsilon_{membrane} = 6$, membrane thickness = 6 nm, $\sigma_{int} = 0.53$ S/m, $\sigma_{membrane} = 0$ µS/m) in a 0.04 S/m medium (d).

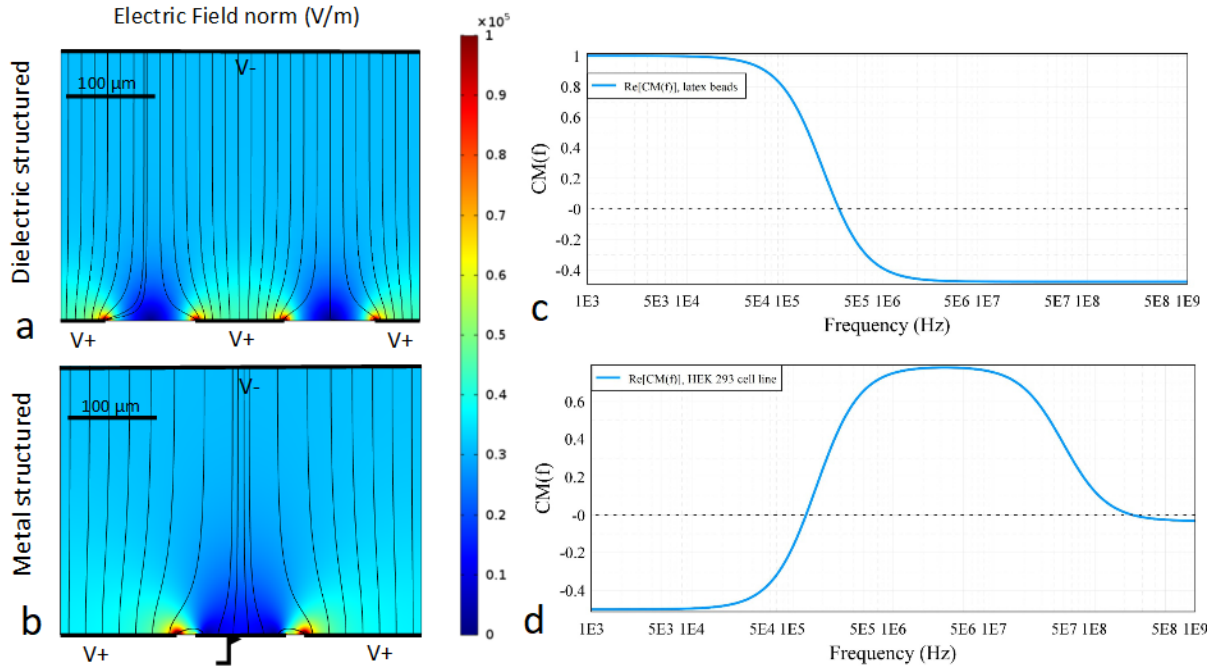

Figure 3: Norm of the electric field for the two top-bottom electrodes design studied (a, b) and for 25 µm wide interdigitated coplanar electrodes separated by a 50 µm gap (c) where voltage was set to 10 V_{pp}. A relative buffer permittivity of 78 was used in each model. Results of the COMSOL particle tracing temporal study with a 10 V_{pp} voltage and the same single shell electrical parameter than previously (d, e, f). Comparison of the particle trapping efficiency for nDEP and pDEP top-bottom designs, and for interdigitated electrodes extracted from the COMSOL temporal study (g).

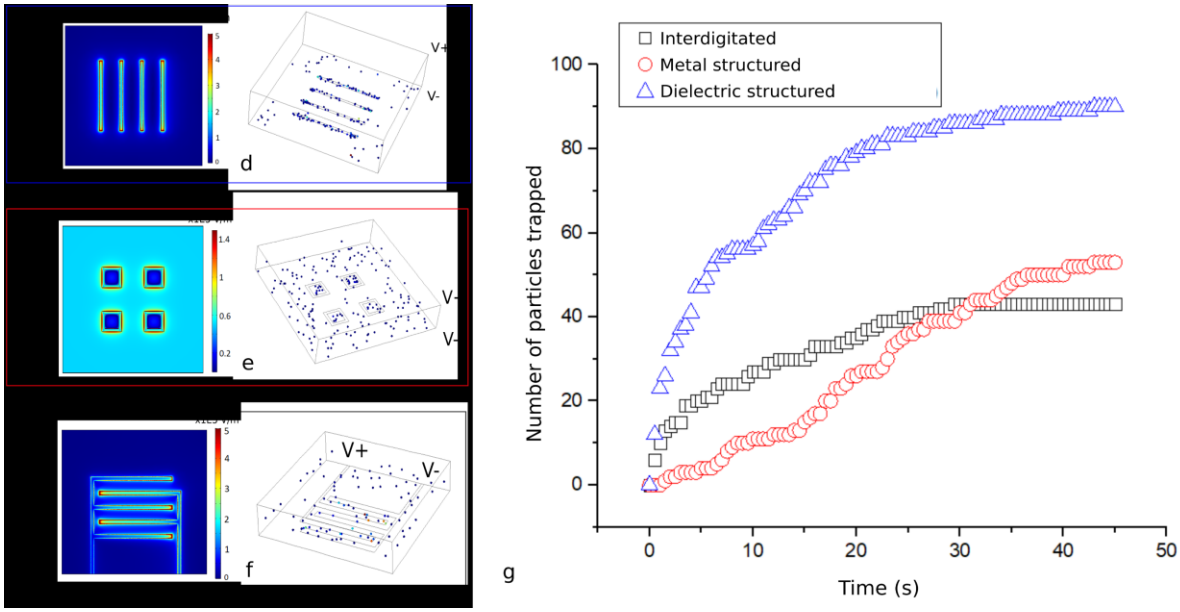

Figure 4: Microscopy image of latex beads trapped by ACEO at 1 kHz and 1Vrms (a). Image of the beads organization when a voltage is applied (b). SPR image of gold electrodes obtained by openings in SiO_2 (c). Dark zones correspond to gold. SPR signal versus time (d) measured on electrodes for DI water and bead solutions at different concentrations C.

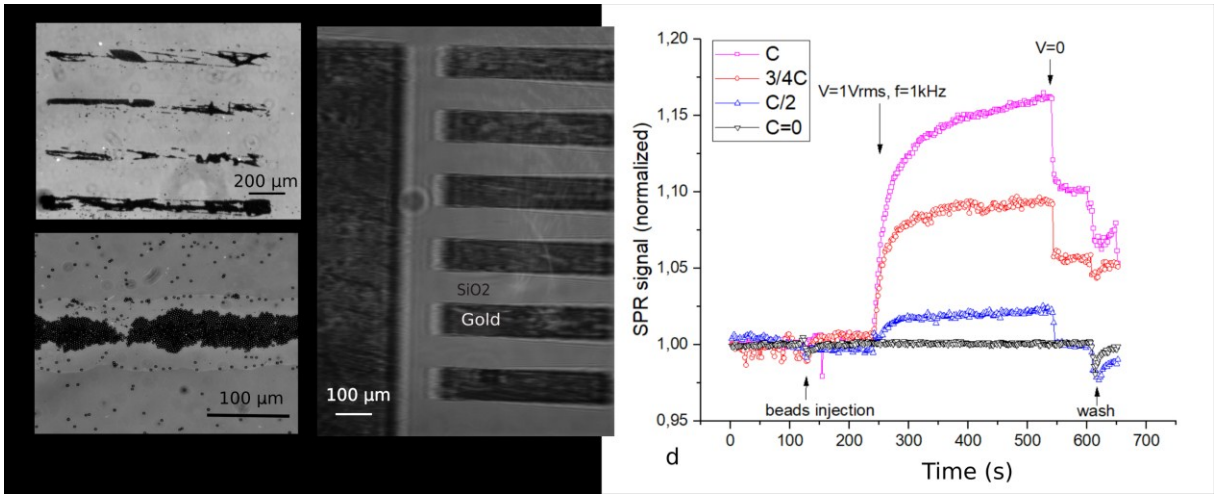

Figure 5: Microscopy image of HEK293 cells trapped by nDEP on isolated gold squares at 7 V_{pp} and 5 kHz (a). SPR image of the patterned zones and of the reference electrode (b). SPR signal versus time on the reference electrode and the DEP electrodes (c).